Limited-view photoacoustic imaging based on an iterative adaptive weighted filtered backprojection approach

Xueyan Liu,[1] Dong Peng,[3] Xibo Ma,[2] Wei Guo,[4] Zhenyu Liu,[2] Dong Han,[2] Xin Yang,[2] and Jie Tian[1,2,*]

[1]Sino-Dutch Biomedical and Information Engineering School of Northeastern University, Shenyang 110004, China

[2]Key Laboratory of Molecular Imaging and Functional Imaging, Institute of Automation, Chinese Academy of Sciences, Beijing 100190, China

[3]Life Sciences Research Center, School of Life Sciences and Technology, Xidian University, Xi'an 710071, China

[4]College of Electronic Information & Control Engineering, Beijing University of Technology, Beijing 100124, China

*Corresponding author: tian@ieee.org

Received 23 January 2013; revised 15 March 2013; accepted 4 April 2013; posted 23 April 2013 (Doc. ID 183931); published 14 May 2013

An iterative adaptive weighted filtered backprojection (FBP) approach was applied to our photoacoustic imaging (PAI) of the optical absorption in biological tissues from limited-view data. By using an image-based adaptive weighted PAI reconstruction, we can modify the defect of the artifacts degrading the quality of the image. Results of numerical simulations demonstrated that the proposed algorithm was superior to FBP in terms of both accuracy and robustness to noise. Reconstructed images of biological tissues agreed well with the structures of the samples. The resolution of the PAI system with the proposed method was experimentally demonstrated to be better than 0.14 mm. By using the proposed method, the imaging quality of the PAI system can be improved.

OCIS codes: (100.3010) Image reconstruction techniques; (110.5120) Photoacoutic imaging.
http://dx.doi.org/10.1364/AO.52.003477

1. Introduction

Photoacoustic imaging (PAI) combining strong optical contrast and high ultrasonic resolution in a single modality has great potential for a wide range of biomedical imaging applications [1], including vessel imaging, cancer detection, and brain imaging [2–4]. Many algorithms have been developed in both the frequency domain and time domain to exactly or approximately reconstruct the image with full-view detection [5]. A limiting factor for these algorithms is the great number of measurements made with transducers, implying long acquisition times. In addition, due to the scattering or reflection of the complex structures in tissues, it is almost impossible to collect the signals from all directions in many practices.

To satisfy the needs of a clinical diagnosis, sparse data techniques for limiting the number of views have been developed [6–15]. Generally, iterative reconstruction algorithms can substantially reduce the number of measurement angles required [6–9]. An image can be reconstructed from far fewer measurements than what the Shannon sampling theory requires if the image is sparse or can be compressed [10–12]. Another approach is to apply analytical methods to expand the data set by extrapolation of the missing data from the reference data set [13–15]. All of these methods provide the opportunity

1559-128X/13/153477-07$15.00/0

for accurate image reconstruction from incomplete measurement data.

In this study, inspired by the effective scanning angle [16,17] and the adaptive iterative reconstruction in computed tomography (CT) [18,19], we derived an iterative adaptive weighted reconstruction scheme for improving image quality in limited-view PAI. The proposed method can compensate for artifacts due to the nonexactness of the backprojection and improve the reconstructed intensity error problem with a limited-view scanning trajectory. During the reconstruction, the effective scanning angle weighted filtered backprojection (FBP) method was used to reconstruct an initial image of the energy deposition. For compensation of the nonexactness of backprojection, the difference between the practical signals and the image-based weighted calculated signals was used to update the correction image in each iteration step [20]. We call this combined iterative reconstruction scheme the iterative adaptive weighted FBP (IAWFBP) approach. This method can reduce artifacts and yield better results with incomplete data and noisy data that reduce the exactness and stability of the reconstruction.

The organization of this paper is as follows. Section 2 introduces the proposed IAWFBP approach briefly. In Section 3, besides the numerical simulations of image reconstruction, we also conducted experimental measurements on biological tissues and applied the proposed method to the obtained data. The final section presents our conclusions.

2. Methods and Materials

A. Iterative Adaptive Weighted Filtered Backprojection Method

In this section, we will present the IAWFBP method for the limited-view PAI image reconstruction. Here we assume that the tissue for imaging is acoustically homogeneous, so the effect of heat conduction in the photoacoustic wave equations can be ignored. Then the acoustic pressure $p(r_0,t)$ can be obtained by using Green's function, providing the forward problem [21]

$$p(r_0,t)=\frac{\beta}{4\pi C_p}\iiint\frac{A(r)}{|r_0-r|}\frac{\partial I(t')}{\partial t'}\mathrm{d}^3r\Big|_{t'=t-|r_0-r|/c},\quad(1)$$

where $p(r_0,t)$ is the acoustic pressure wave at position r_0 and time t; c is the sound speed; β is the thermal expansion coefficient; C_p is the specific heat; $A(r)$ is the absorbed energy deposition; and $I(t')$ is the temporal profile. For two-dimensional circular scanning, the PAI inverse problem of Eq. (1) is to recover $A(r)$ from the measurements of the pressure $p(r_0,t)$ detected by a transducer [22]:

$$A(r)=-\frac{r_0^2C_p}{2\pi\beta c^4}\int_{\varphi_0}\mathrm{d}\varphi_0\frac{1}{t}\frac{\partial p(r_0,t)}{\partial t}\Big|_{t=|r_0-r|/c}.\quad(2)$$

To numerically model the above forward and inverse problems, we used vector x to represent $A(r)$ and vector y to represent $p(r_0,t)$. Then, the exact forward problem can be described as $y=\Phi x$, and the exact reconstruction formula can be written as $\Psi\Phi x=x$, where Ψ represents the exact backprojection operator.

In much actual biological tissue imaging, only the noisy photoacoustic signals can be detected in a limited view. Φ is an ill-conditioned matrix, which means $\Psi\neq\Phi^{-1}$. Thus we cannot obtain an exact image. For the two-dimensional incomplete case by using the weighted effective scanning angle, the algorithm for full-view data can be approximately extended to the limited-view case. The reconstructed intensity error problem induced by the limited view can be improved [16,17]:

$$A(r)\approx-\frac{r_0^2C_p}{2\pi\beta c^4}\int_{\theta_1}^{\theta_2}\mathrm{d}\theta_0\frac{1}{\theta_e t}\frac{\partial p(r_0,t)}{\partial t}\Big|_{t=|r_0-r|/c},\quad(3)$$

where θ_1 and θ_2 are, respectively, the minimum and maximum angle of the signal acquisition position; θ_e is the effective scanning angle of the reconstructed position. Based on Eq. (3), we used the proposed method to compensate for the nonexactness of the backprojection.

The IAWFBP algorithm is designed to reconstruct the absorbed energy deposition by minimizing the error between the practical image and the reconstructed image. First, an initial image x_0 was reconstructed by the weighted FBP method. To compensate the difference between the initial image and the practical image, based on the image x_0, a weighted parameter

$$\lambda_1=\frac{\max(y)-\min(y)}{\max(x_0)-\min(x_0)}\quad(4)$$

was used to correct the differences between the measured signals y and computed signals Φx_0. We obtained the correction image Δx_1 from the differences between y and $\lambda_1\Phi x_0$. The updated step is given by

$$x_1=x_0+\alpha\Delta x_1=x_0+\alpha\Psi(y-\lambda_1\Phi x_0).\quad(5)$$

In practice, it might be wise to employ only a fraction $\alpha\in(0,1)$ of the full values of the correction image Δx_1, and this condition assumption is useful to prevent overcorrection. By using an image-based adaptive weighted

$$\lambda_i=\frac{\max(y)-\min(y)}{\max(x_i)-\min(x_i)}\quad(6)$$

in the calculation of an error correction image at each iteration step, the recursion expression is as follows:

$$x_i = x_{i-1} + \Delta x_i = x_{i-1} + \alpha\Psi(y - \lambda_i \Phi x_{x_{i-1}}),$$
$$i = 1, 2, \cdots. \tag{7}$$

The reciprocal of the number of elements was used to represent a weighting factor in the conventional iterative reconstruction algorithm [23,24]. In this study, we used an image-based adaptive weight parameter λ_i to correct the differences between the measured signals and the computed signals. No normalization with the number of elements was used, and consequently no energy conservation was obtained with the reconstruction. However, the error between the measured signals y and computed signals $\lambda_i \Phi x_0$ became smaller with repeated iterations until the image converged. This is the main difference with the conventional iterative algorithm.

We have not been able to give a formal proof that such projection signals are useful. If the system converges, the difference between the practical image and the reconstructed image should become smaller and smaller for each iteration. In this paper, the normalized mean absolute error (NMAE) that is most sensitive to distortion artifacts is defined as

$$\delta_i = \|x_i - x\|_2 / \|x\|_2. \tag{8}$$

The best algorithm will have a minimum value of NMAE. The iterative process will stop when a desired minimum NMAE has been achieved, and then the reconstruction results will be output.

B. Imaging System

The schematic of the experimental setup is shown in Fig. 1, where a laboratory coordinate system $[x, y, z]$ is also depicted. A Q-switched Nd:YAG loaser operated at 532 nm with repetition rate at 10 Hz was used as the light source. The laser beam was expanded and homogenized to provide an incident energy density of <20 mJ/cm^2. An unfocused needle hydrophone (Precision Acoustics Ltd.) with a diameter of 1 mm and frequency response of 500 kHz–15 MHz was

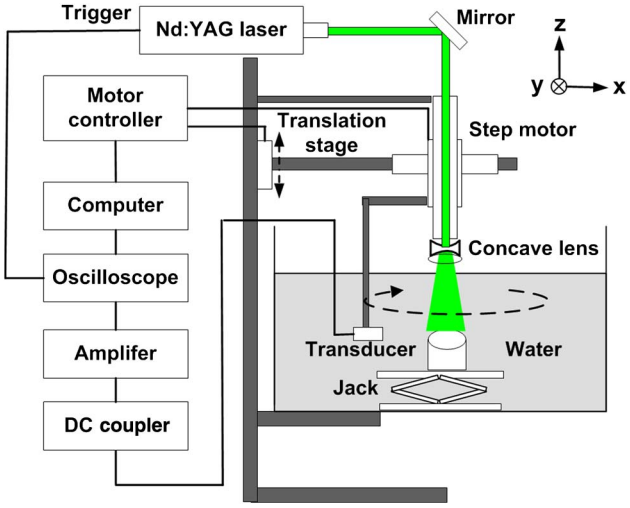

Fig. 1. Experimental setup for PAI signal detection.

controlled by a high-precision stepping motor to scan around the sample in a circular manner in the horizontal x–y plane for photoacoustic signal acquisition. The distance between the transducer and the rotation center was 45 mm. At each detection position, the PAI signals were first amplified through a pulse amplifier, then recorded and averaged 50 times by a digital oscilloscope (MSO4000B, Tektronix), and finally transferred to a personal computer for subsequent data processing and imaging.

3. Results

A. Limited-view Numerical Simulations

The numerical simulation was used to evaluate the above algorithm. The simulation samples of four cylinders composed of uniform disks possessing different gray levels, radii, and locations were used as the given initial energy deposition (Table 1). The simulated acoustic wave was calculated according to Eq. (1). In the simulations, the radius of the detection circle was 30 mm, the imaged field measuring 21 mm × 21 mm was mapped with a 256 × 256 mesh, and the center of S1 was positioned at the origin of the circle of detection.

Images reconstructed with the FBP method, the algebraic reconstruction technique-FBP (ART-FBP) [25,26] method, and the IAWFBP method from limited-angle data are displayed in the first, second, and third rows of Fig. 2, respectively. One can see that there are serious artifacts and blurs in the first row. These artifacts will limit the spatial resolution and degrade image contrast. By using the ART-FBP method, the artifacts of FBP can be reduced effectively and the quality of the reconstructed image can be improved greatly. There are fewer artifacts and blurs in the image reconstructed by the IAWFBP method. By adopting a more accurate model, the proposed method can effectively suppress streak artifacts in the background and improve the detailed information of the reconstruction.

The first column of Fig. 2 was reconstructed with data collected from 30 positions over 90° in the first quadrant. Since the detection view is insufficient, one can identify that the parts of the inclusion boundaries in the second and fourth quadrants are affected and distorted. This result is in agreement with the theoretical prediction in [6]. The second and third columns employed the data collected from 60 detectors over 135° and 120 detectors over 180°. Notice that the quality of images in these two rows is much better. All the boundaries of the inclusions in the chord are sharply reconstructed. Images

Table 1. Analytical Circles Numerical Phantom Parameters

Target	Center location (mm)	Radius (mm)	Absorption (AU)
S1	(0, 0)	10	0.3
S2	(−3, 3)	1	0.5
S3	(3, 3)	1	0.75
S4	(0, −3)	1.5	1

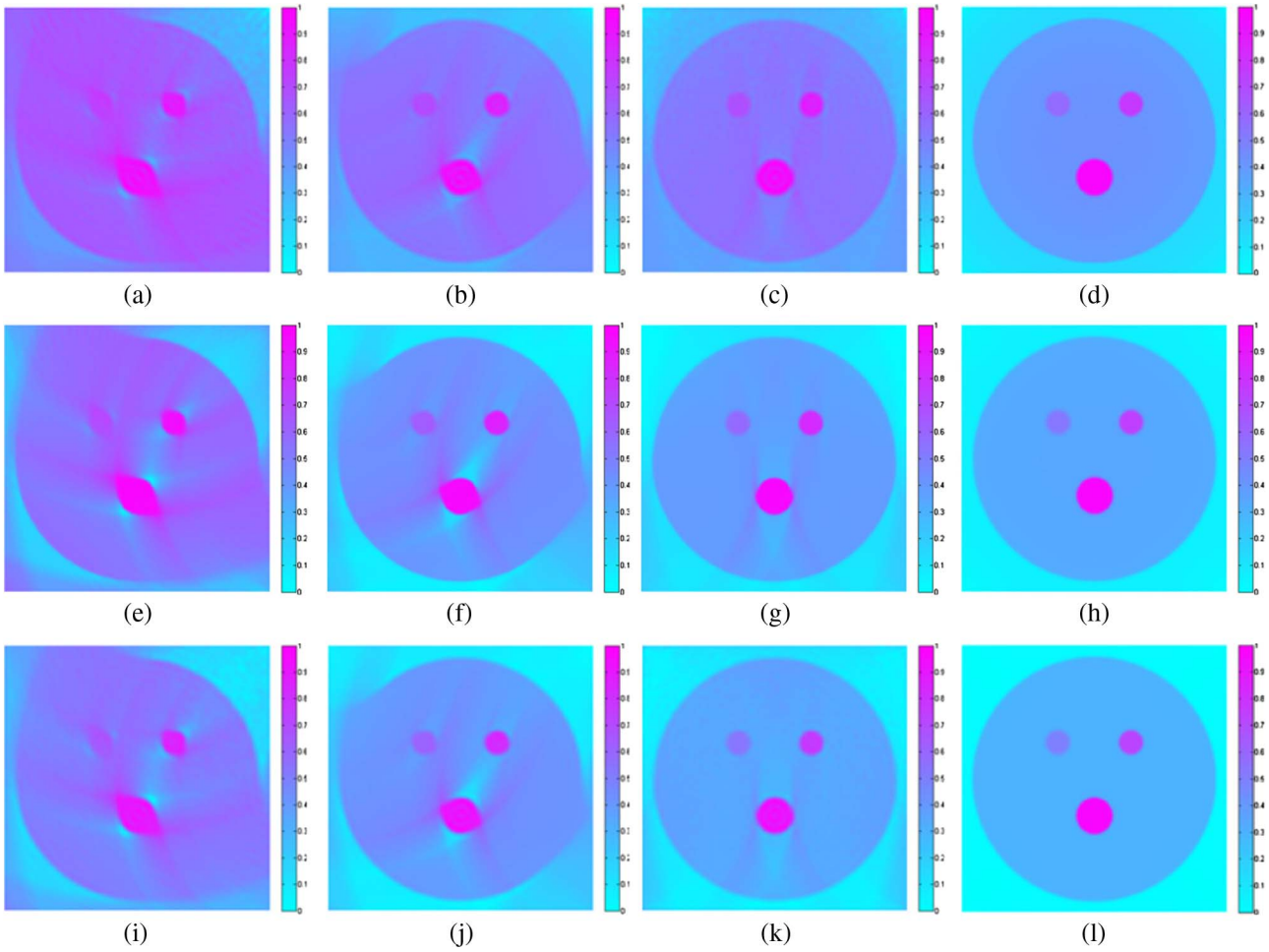

Fig. 2. Images reconstructed from simulated data corresponding to the numerical phantom using (a) 30 detectors over 90°, with FBP; (b) 60 detectors over 135°, with FBP; (c) 120 detectors over 180°, with FBP; (d) 240 detectors over 360°, with FBP; (e) 30 detectors over 90°, with ART-FBP; (f) 60 detectors over 135°, with ART-FBP; (g) 120 detectors over 180°, with ART-FBP; (h) 240 detectors over 360°, with ART-FBP; (i) 30 detectors over 90°, with IAWFBP; (j) 60 detectors over 135°, with IAWFBP; (k) 120 detectors over 180°, with IAWFBP; (l), 240 detectors over 360°, with IAWFBP.

reconstructed from the full-view data using the three methods are displayed in the last column of Fig. 2.

To demonstrate the accuracy of the IAWFBP algorithm, with a different total number of detection positions, the NMAEs between the original image and the reconstructed images were calculated and are shown in Fig. 3(a). Compared with the FBP method and the ART-FBP method, the proposed method has greater improvement in calculation accuracy. In addition, NMAE decreases especially when there are fewer detection positions. It seems that 60 detection positions are more than enough for good reconstruction when the scanning angle is 180°. To demonstrate the robustness to noise of the IAWFBP algorithm, photoacoustic signals were polluted with various levels of white Gaussian noise. Figure 3(b) displays the tendency chart of the NMAEs in reconstructed images with the IAWFBP method under three conditions. From Fig. 3(b) we can conclude that the proposed method is robust to inaccurate measurements.

B. PAI of the Phantom

In the first experiment, a cylindrical turbid phantom made of a mixture with 1% intralipid, 6% gelatin, and 93% water was used to simulate biological tissues. The phantom shown in Fig. 4(a) contained two graphite rods with the same radius $r = 0.25$ mm. The targets were buried in the cylindrical phantom at a depth of 4 mm, and the distance between them was 3.5 mm. The induced photoacoustic waves were captured at 120 positions over 360°. In real experiments, we did not know the true image, so the iterative stop criteria

$$e_i = \|x_i - x_{i-1}\|_2 / \|x_i\|_2 < \varepsilon, \qquad (i = 1, 2, \cdots n)$$

was taken.

Images reconstructed from limited-view data and full-view data of the phantom are shown in the first and second rows of Fig. 4, respectively. As expected, reconstructions with the FBP method contain many artifacts and distortions, and those artifacts are

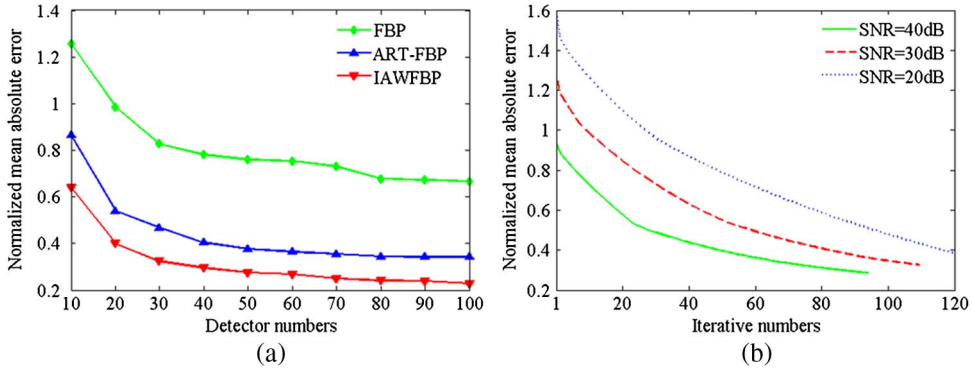

Fig. 3. Reconstruction NMAE (a) from 180° with a different total number of detection positions and (b) from 60 detectors over 180° noisy observation with different SNR.

reduced when using the ART-FBP method, while the image reconstructed with the IAWFBP approach provides high-quality images.

To evaluate the spatial resolution of the reconstruction images with the IAWFBP algorithm, a reconstructed normalization line profile at position $y = 10.52$ mm of the image in Fig. 4(f) is shown in Fig. 5. According to the Rayleigh criterion [27,28], the minimum distinguishable distance between two graphite absorbers is approximately $R = |BC| + |DE| - 2r$. The detectable frequency band of the transducer was from 5 KHz to 15 MHz. With a lower cutoff frequency the spatial resolution of the detector system became lower, and only the signal with a sufficiently high frequency could restore good spatial resolution. A modified ramp filter with a cutoff frequency of 6 MHz was our choice in the reconstruction. Therefore, the estimated highest spatial resolution was 0.125 mm. The result in Fig. 5 shows that with the IAWFBP algorithm we can achieve a spatial resolution of 0.14 mm.

C. PAI of Biological Tissues

In the biological tissue experiment, three circles of pork liver slices buried 3 mm deep in the fresh pork fat slab were adopted as the adsorption objects. The pork liver slices had a thickness of about 1 mm and diameter of about 1 mm in the imaging plane, respectively. We used 1.5 mm/μs as the estimated sound velocity in soft tissues. With a scanning radius of 45 mm, photoacoustic data were collected around the sample over a 2π angular span with 120 steps. Image reconstruction utilized the IAWFBP algorithm described in Eq. (7).

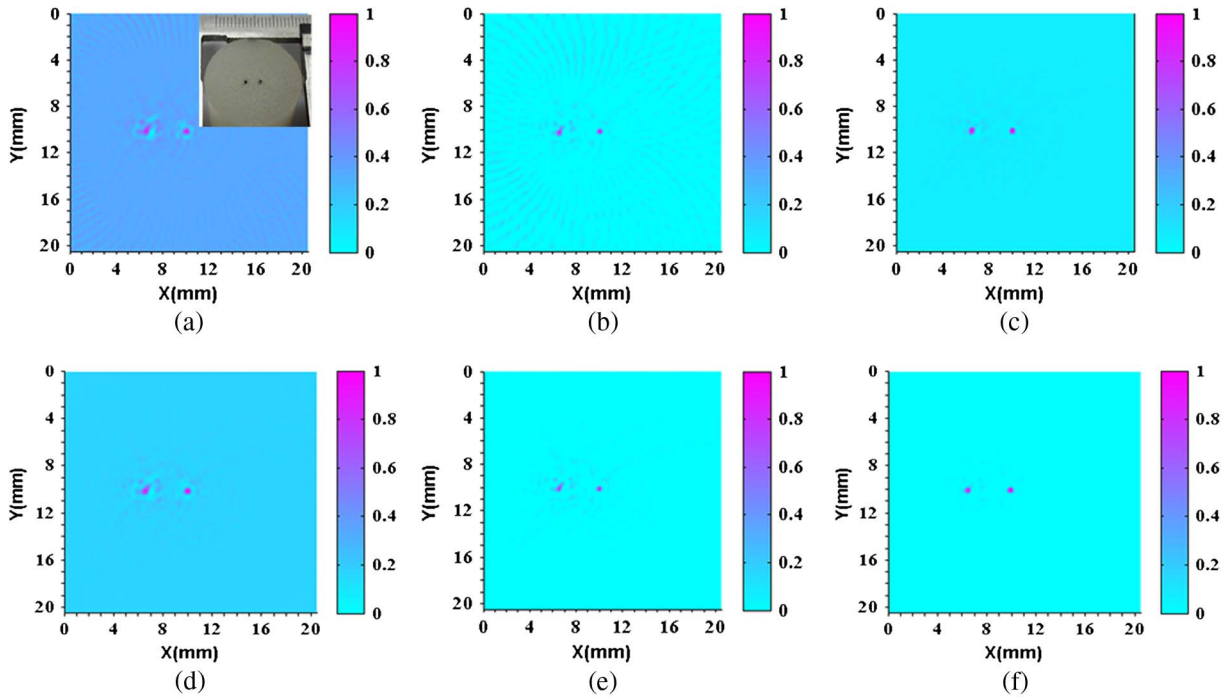

Fig. 4. Reconstructed photoacoustic images based on few-detector data. (a) 60 detectors over 180°, with FBP. The insert at the top-right corner is the photograph of the phantom. (b) 60 detectors over 180°, with ART-FBP. (c) 60 detectors over 180°, with IAWFBP. (d) 120 detectors over 360°, with FBP. (e) 120 detectors over 360°, with ART-FBP. (f) 120 detectors over 360°, with IAWFBP.

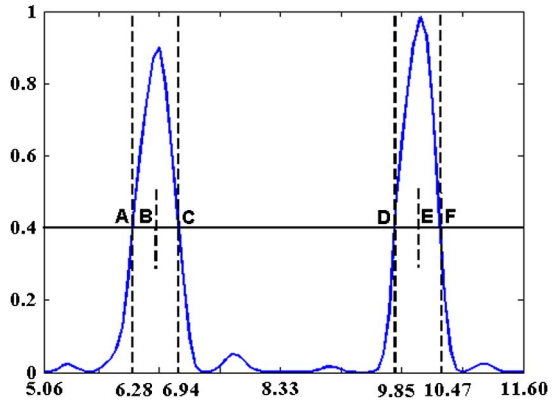

Fig. 5. Center line profile of the reconstructed image shown in Fig. 4(f) with $y = 10.52$ mm.

Figures 6(a)–6(c) show the images reconstructed using the FBP method, the ART-FBP method, and the IAWFBP method, respectively, with limited-view data from 60 detectors over 180°. We can see serious intensity fluctuations around the pork livers, which come mainly from the photoacoustic signals generated in the background pork fat tissues. By comparing those three images, one can find that considerably improved images were reconstructed using the IAWFBP approach. All boundaries of the pork livers in Fig. 6(c) were sharper, and the quality of the reconstruction was satisfactory.

Figures 6(d) through 6(f) display the reconstructions using the FBP method, the ART-FBP method, and the IAWFBP method, respectively, with data from 120 detectors over 360°. Based on our PAI system as well as the IAWFBP reconstruction algorithm, the full-view data reconstruction shown in Fig. 6(f) is almost perfect. The highly absorbing pork livers in the pork fat with comparatively low absorption were well localized. The shapes and sizes of the three pork livers were imaged well compared with the picture of the biological tissues. Because both the pork livers and fat are soft biological tissues, the shapes of the pork livers in Fig. 6(f) have minor discrepancies with those appearing in the photographs. However, their relative positions were not altered.

4. Discussion and Conclusion

An iterative adaptive weighted algorithm has been applied to reconstruct the deposition of optical absorbed energy from pressure signals detected in a limited view. The major advantage of this method is that it can greatly reduce the artifacts and associated blurs caused by the iteration process in the case that data sets are incomplete or noisy. By comparing Figs. 6(c) and 6(f), the quality of the images reconstructed from incomplete data is comparable with that from full-view data. Scanning a smaller range has the advantage of reducing the scanning time or the size of the acoustic transducer array. However, due to a limited view, artifacts and blurs still appear in the reconstruction. It is worth mentioning that the reconstruction time for a 256 × 256 grid using the proposed method is several minutes, which is one limitation of the proposed method. The calculation time would be decreased greatly by using a regularization-based PAI algorithm [29]. The relatively long scanning time is still one limitation of this system. By

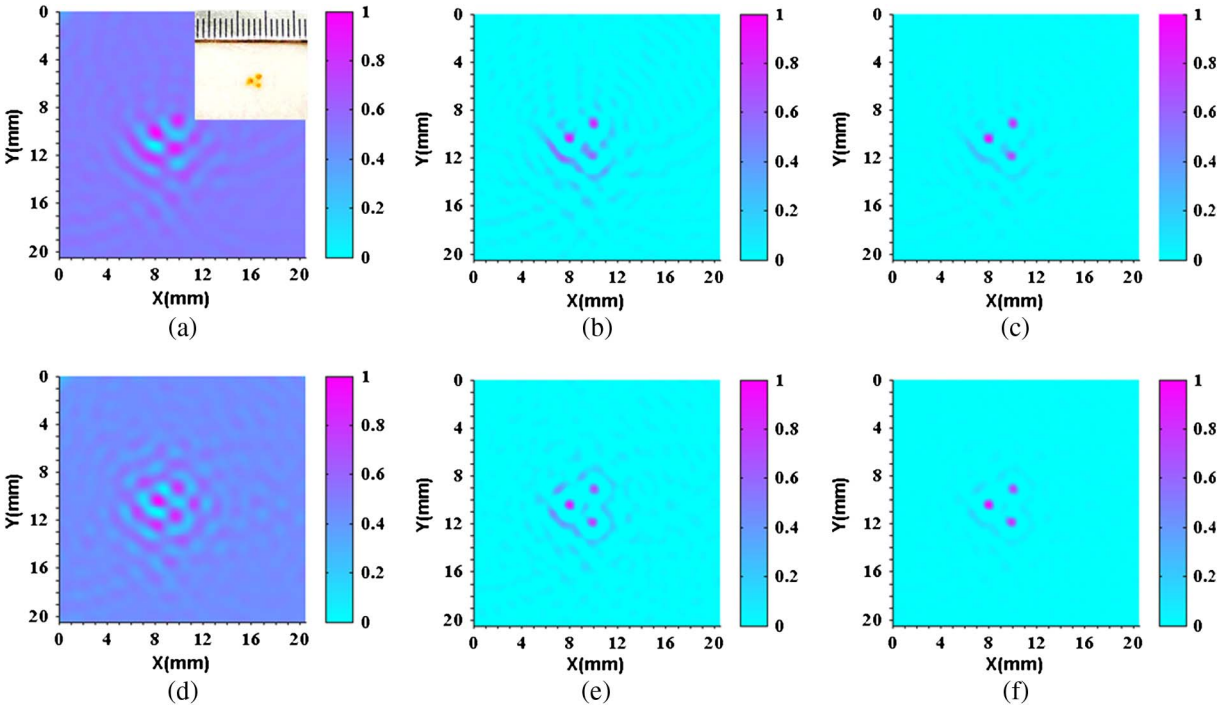

Fig. 6. PAI of three slices of pork livers that were buried 3 mm deep in a pork fat slab. (a) 60 detectors over 180°, with FBP. The insert at the top-right corner is the picture of the imaged biological tissues. (b) 60 detectors over 180°, with ART-FBP. (c) 60 detectors over 180°, with IAWFBP. (d) 120 detectors over 360°, with FBP. (e) 120 detectors over 360°, with ART-FBP. (f) 120 detectors over 360°, with IAWFBP.

using a multielement transducer array along with higher pulse-repetition-rate multispectral lasers, the scanning time can be reduced greatly [30].

In summary, we have presented a feasibility study on the application of an IAWFBP algorithm to reconstruct photoacoustic images with limited-view data. The experiments and simulations demonstrated that the IAWFBP approach can improve the accuracy and contrast of the reconstruction images compared with the FBP method. Reconstructed images of two graphite rods embedded in a turbid phantom and three pork livers buried in a pork fat slab agree well with the pictures of the samples. The NMAE calculation also denoted that the IAWFBP algorithm has an advantage in accuracy. Therefore, it can be a promising candidate for resolving the limited-view PAI problem.

This paper is supported by the National Basic Research Program of China (973 Program) under Grant 2011CB707700; the Instrument Developing Project of the Chinese Academy of Sciences under Grant No. YZ201164; the National Natural Science Foundation of China under Grant Nos. 81227901, 61231004, 81027002, 81071205, 81071129, and 81101095; National Key Technology R&D Program under Grants 2012BAI23B01, 2012BAI23B06; the Beijing Natural Science Foundation No. 4111004; the Fellowship for Young International Scientists of the Chinese Academy of Sciences under Grant No. 2010Y2GA03; the Chinese Academy of Sciences Visiting Professorship for Senior International Scientists under Grant Nos. 2012T1G0036, 2010T2G36, 2012T1G0039; and the NSFC-NIH Biomedical collaborative research program under 81261120414.

References

1. L. V. Wang, "Prospects of photoacoustic tomography," Med. Phys. **35**, 5758–5767 (2008).
2. L. V. Wang and S. Hu, "Photoacoustic tomography: in vivo imaging from organelles to organs," Science **335**, 1458–1462 (2012).
3. Z. Yuan, Q. Zhang, E. Sobel, and H. Jiang, "Image-guided optical spectroscopy in diagnosis of osteoarthritis: a clinical study," Biomed. Opt. Express **1**, 74–86 (2010).
4. X. Wang, Y. Pang, G. Ku, X. Xie, G. Stoica, and L. V. Wang, "Noninvasive laser-induced photoacoustic tomography for structural and functional in vivo imaging of the brain," Nat. Biotechnol. **21**, 803–806 (2003).
5. M. Xu and L. V. Wang, "Photoacoustic imaging in biomedicine," Rev. Sci. Instrum. **77**, 041101 (2006).
6. Y. Xu and L. V. Wang, "Reconstructions in limited-view thermoacoustic tomography," Med. Phys. **31**, 724–733 (2004).
7. B. T. Cox, S. R. Arridge, K. P. Kostli, and P. C. Beard, "Two-dimensional quantitative photoacoustic image reconstruction of absorption distributions in scattering media by use of a simple iterative method," Appl. Opt. **45**, 1866–1875 (2006).
8. L. Z. Xiang, D. Xing, H. M. Gu, D. W. Yang, S. H. Yang, and L. Zeng, "Photoacoustic imaging of blood vessels based on modified simultaneous iterative reconstruction techniques," Acta Phys. Sin. **56**, 3911–3917 (2007).
9. C. Tao and X. Liu, "Reconstruction of high quality photoacoustic tomography with a limited-view," Opt. Express **18**, 2760–2766 (2010).
10. J. Provost and F. Lesage, "The application of compressed sensing for photoacoustic tomography," IEEE Trans. Med. Imaging **28**, 585–594 (2009).
11. Z. Guo, C. Li, L. Song, and L. V. Wang, "Compressed sensing in photoacoustic tomography in vivo," J. Biomed. Opt. **15**, 021311 (2010).
12. J. Meng, L. V. Wang, L. Ying, D. Liang, and L. Song, "Compressed-sensing photoacoustic computed tomography in vivo with partially known support," Opt. Express **20**, 16510–16523 (2012).
13. S. K. Patch, "Thermoacoustic tomography: consistency conditions and the partial scan problem," Phys. Med. Biol. **49**, 2305–2315 (2004).
14. J. K. Gamelin, A. Aguirre, and Q. Zhu, "Fast, limited-data photoacoustic imaging for multiplexed systems using a frequency-domain estimation technique," Med. Phys. **38**, 1503–1518 (2011).
15. Z. Yuan and H. Jiang, "A calibration-free, one-step method for quantitative photoacoustic tomography," Med. Phys. **39**, 6895–6899 (2012).
16. G. Paltauf, R. Nuster, and P. Burgholzer, "Weight factors for limited angle photoacoustic tomography," Phys. Med. Biol. **54**, 3303–3314 (2009).
17. D. Wu, C. Tao, X. Liu, and X. Wang, "Influence of limited-view scanning on depth imaging of photoacoustic tomography," Chin. Phys. B **21**, 014301 (2012).
18. M. Magnusson, P. E. Danielsson, and J. Sunnegardh, "Handling of long objects in iterative improvement of nonexact reconstruction in helical cone-beam CT," IEEE Trans. Med. Imaging **25**, 935–940 (2006).
19. H. Bruder, R. Raupach, J. Sunnegardh, M. Sedlmair, K. Stierstorfer, and T. Flohr, "Adaptive iterative reconstruction," Proc. SPIE **7961**, 79610J (2011).
20. R. L. O'Halloran, Z. Wen, J. H. Holmes, and S. B. Fain, "Iterative projection reconstruction of time-resolved images using highly-constrained back-projection (HYPR)," Magn. Reson. Med. **59**, 132–139 (2008).
21. G. J. Diebold, M. I. Khan, and S. M. Park, "Photoacoustic signatures of particulate matter: optical production of acoustic monopole radiation," Science **250**, 101–104 (1990).
22. M. Xu and L. V. Wang, "Universal backprojection algorithm for photoacoustic computed tomography," Phys. Rev. E **71**, 016706 (2005).
23. S. Ma, S. Yang, and H. Guo, "Limited-view photoacoustic imaging based on linear-array detection and filtered mean-backprojection-iterative reconstruction," J. Appl. Phys. **106**, 123104 (2009).
24. G. Paltauf, J. A. Viator, S. A. Prahl, and S. L. Jacques, "Iterative reconstruction algorithm for optoacoustic imaging," J. Acoust. Soc. Am. **112**, 1536–1544 (2002).
25. D. Yang, D. Xing, Y. Wang, Y. Tan, and B. Yi, "Limited-view scanning photoacoustic imaging based on algebraic reconstruction techniques," J. Acta Opt. Sin. **25**, 772–776 (2005).
26. X. Liu, J. Tian, D. Han, W. Guo, D. Peng, X. Ma, C. Qin, and X. Yang, "Effect of iterative reconstruction integrating SART and FBP on photoacoustic imaging," Proc. SPIE **8313**, 83133Z (2012).
27. S. Yang and D. Xing, "Functional imaging of cerebrovascular activities in small animals using high-resolution photoacoustic tomography," Med. Phys. **34**, 3294–3301 (2007).
28. X. Wang, Y. Xu, and M. Xu, "Photoacoustic tomography of biological tissues with high cross-section resolution: reconstruction and experiment," Med. Phys. **29**, 2799–2801 (2002).
29. L. Yao and H. Jiang, "Photoacoustic image reconstruction from few-detector and limited-angle data," Biomed. Opt. Express **2**, 2649–2654 (2011).
30. A. Taruttis, S. Morscher, N. C. Burton, D. Razansky, and V. Ntziachristos, "Fast multispectral optoacoustic tomography (MSOT) for dynamic imaging of pharmacokinetics and biodistribution in multiple organs," PLos ONE **7**, e30491 (2012).